Atmospheric Research 247 (2021) 105152

Contents lists available at ScienceDirect

Atmospheric Research

journal homepage: www.elsevier.com/locate/atmosres

# Change in the heatwave statistical characteristics over China during the climate warming slowdown

Xin Li[a,b], Guoyu Ren[c,d,*], Suyan Wang[b], Qinglong You[a,e], Yinchuan Sun[b], Yang Ma[b], Dai Wang[b], Wen Zhang[b]

[a] Key Laboratory of Meteorological Disaster, Ministry of Education (KLME)/Joint International Research Laboratory of Climate and Environmental Change (ILCEC)/ Collaborative Innovation Center on Forecast and Evaluation of Meteorological Disasters (CIC-FEMD)/Earth System Modeling Center, Nanjing University of Information Science and Technology (NUIST), Nanjing, China

[b] Key Laboratory of Meteorological Disaster Monitoring and Early Warning and Risk Management of Characteristic Agriculture in Arid Regions, CMA, Yinchuan, China

[c] Department of Atmospheric Science, School of Environmental Studies, China University of Geosciences, Wuhan, China

[d] Laboratory for Climate Studies, National Climate Center, CMA, Beijing, China

[e] Department of Atmospheric and Oceanic Sciences & Institute of Atmospheric Sciences, Fudan University, Shanghai, China

ARTICLE INFO

*Keywords:*
Warming slowdown
Heatwaves
Joint probability distribution
Joint return period
China

ABSTRACT

Heatwaves are multi-day periods of extremely high-temperature weather relative to a region's average conditions and are among the deadliest natural disasters. This study was designed to evaluate changes in the characteristics of heatwaves during the periods of warming acceleration versus warming slowdown using the multivariate joint probability distributions of heatwave duration and severity. The results revealed that: (1) From the warming acceleration period (1961–1997) to the warming slowdown period (1998–2017), the return levels of heatwave duration increased by < 1.0 d as the return period increased. As the return period lengthened, the return level of heatwave severity rose as well; (2) The joint occurrence probability of heatwaves with both variables exceeding the 20-yr, 50-yr, and 100-yr return levels exhibited relative increases of 3%, 8%, and 16% across China, respectively. There were greater than the joint probability of heatwaves with only 1 variable exceeding the return levels; (3) The number of heatwaves with both duration and severity exceeding the 50-yr joint return period increased in China, and this increase was dominated by heatwaves with joint return periods of 50–100 years, leading to a strengthening of heatwave severity.

## 1. Introduction

Heatwaves are extreme climatic events featuring continuous high-temperature weather conditions that exert significant negative impacts on human health, urban air quality, ecological and environmental conditions. Against the backdrop of global warming, the duration of extremely hot weather is expected to continue increasing (Baldwin et al., 2019). For instance, since the deadly heatwaves of 2003 and 2010, Europe has experienced a growing number of hot summers, with an observed summer temperature increase of 0.81 °C since 2003, a trend that has overburdened the ecological and public health systems (Christidis et al., 2014 Teuling, 2018). Consequently, heatwaves have become the primary indicator used in assessing the impact of climate change (Jones et al., 2018 Tebaldi and Lobell, 2018 Warshaw, 2018). Studies have shown that under the conditions of continued global warming, populations living in developing countries will face a higher risk of being influenced by heatwaves, public health will be more severely impacted by simultaneously high temperatures and humidity levels, and humid tropical areas will tend to experience more frequent heat stress than other regions (Luo and Lau, 2019 Russo et al., 2019 Zhao et al., 2015). By 2100, nearly half the world's population may be impacted by fatal heatwaves every year (Mora et al., 2017).

There is currently no unified definition of heatwaves. Whether defined by an absolute or relative threshold value, under the combined effects of global warming and rapid urbanization, heatwaves in most parts of China have been increasing since the 1990s, especially along the southeastern coast and in North China (Ding et al., 2009 Luo et al., 2020 Yang et al., 2018 You et al., 2017). Significant increases in heatwave frequency, days, and duration were observed in southern China from 1979 to 2010 (Luo and Lau, 2017). Since the early 1950s, anthropogenic influences have caused a more than 60-fold increase in the likelihood of events such as the extremely warm summer of 2013 in

* Corresponding author at: Department of Atmospheric Science, School of Environmental Studies, China University of Geosciences, Wuhan, China.
*E-mail address:* guoyoo@cma.gov.cn (G. Ren).

https://doi.org/10.1016/j.atmosres.2020.105152
Received 30 March 2020; Received in revised form 19 July 2020; Accepted 20 July 2020
Available online 23 July 2020
0169-8095/ 

eastern China, a trend that is projected to continue (Sun et al., 2014). Urbanization accounts for nearly 30% of the increase in mean and extreme heat stress, and the effects of urbanization are more prominent in major urban conglomerates such as Beijing-Tianjin-Hebei and the Yangtze and Pearl river deltas (Luo and Lau, 2018). The rise of the global average temperature has slowed since 1998 (Fyfe et al., 2016 Medhaug et al., 2017), and the warming trend has also slowed in northern China, particularly in Northeast China (Sun et al., 2018). Nonetheless, during the climate-warming slowdown period, it has become hotter in summer but colder in winter in northern China (Li et al., 2015).

The characteristic indicators of heatwaves are their frequency, severity, and duration. In previous studies on heatwaves, these indicators have been used as independent variables for analysis (Wehner et al., 2018), and it was assumed that the marginal distribution function of a single variable conformed to a certain type. For instance, Wang et al. (2016) used the generalized extreme value (GEV) model to study the probability characteristics of extreme temperature in the United States in January and July, while giving less consideration to the interconnection between different variables. Due to its advantage of connecting multiple variables subject to any marginal distribution to obtain a multivariate joint distribution function and effectively describing the correlation structure between variables, the Copula function has gained increasing attention in the research fields of the hydrological process, meteorological drought, and extreme precipitation (Kao and Govindaraju, 2008 Shiau and Modarres, 2009 Yan, 2006).

Based on Copulas, Jeong et al. (2014) found that the future marginal values of flood characteristics and the multivariate joint probability of floods corresponding to longer return periods will be more affected by anthropogenic climate change than those corresponding to shorter return periods. Cheng et al. (2016) applied Copulas to analyze the drought characteristics of California, in different periods. Zhou and Liu (2018) examined the likelihood of concurrent extreme temperature and precipitation modes at the interannual scale, including compound cool/dry and cool/wet events during the cold season, as well as compound hot/dry and hot/wet events during the warm season using Copulas. In a study on heatwaves by Mazdiyasni et al. (2019), the Copula was introduced to construct a multivariate curve of severity, duration, and frequency of heatwaves in 6 cities of the United States, finding that in Los Angeles, greenhouse gas emissions increased the likelihood of heatwaves (4 consecutive days with temperatures exceeding 31 °C) by 21%.

The main objective of this study was to evaluate changes in the characteristics of heatwaves in China from 1961 to 2017. The return levels of heatwave duration and severity were investigated using conventional univariate analysis, and the joint occurrence probabilities of heatwave duration and severity based on Copulas were compared during 2 periods, the warming acceleration period (1961–1997) and the warming slowdown period (1998–2017). The possible causes of the differences between these periods were discussed, with the hope of improving understanding of the variation characteristics of regional heatwaves and providing useful information for assessing the impact and risk of heatwaves.

## 2. Data and study area

The data used in this study were extracted from the daily maximum temperature observations collected by 769 meteorological stations across China from 1961 to 2017. The data were qualified and homogenized by the China National Meteorological Information Center of the China Meteorological Administration (CMA). Considering the completeness and continuity of the historical sequence, we removed the meteorological stations that failed to measure the daily maximum temperature for more than 1 month and those which had not detected a protracted period of high temperatures lasting more than 3 days. Ultimately, 673 stations were selected, and their distribution is shown in Fig. 1. The meteorological stations are densely distributed in the eastern monsoon region, with fewer stations unevenly distributed in the Qinghai-Tibet Plateau and the desert area in southern Xinjiang.

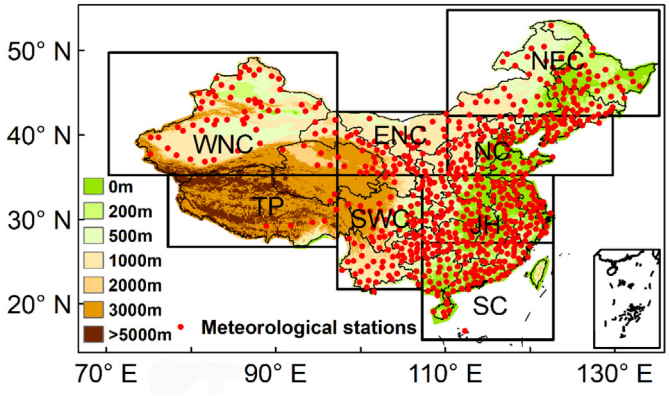


**Fig. 1.** Distribution of meteorological stations and boundaries of 8 subregions in the study area.

**Table 1**
Coordinates of the subregions.

| Subregion | Latitude | Longitude |
|---|---|---|
| All of China (CN) | 15.75–54.75°N | 70.25–135.25°E |
| Northeast China (NEC) | 42.25–54.75°N | 110.25–135.25°E |
| North China (NC) | 35.25–42.25°N | 110.25–129.75°E |
| Jiang-Huai (JH) | 27.25–35.25°N | 107.25–122.75°E |
| South China (SC) | 15.75–27.25°N | 107.25–122.75°E |
| Southwest China (SWC) | 21.75–35.25°N | 97.25–107.25°E |
| Tibetan Plateau (TP) | 26.75–35.25°N | 77.25–97.25°E |
| Western Northwest China (WNC) | 35.25–49.75°N | 70.25–97.25°E |
| Eastern Northwest China (ENC) | 35.25–42.75°N | 97.25–110.25°E |

Based on relevant literature, we divided China into 8 subregions (Table 1) (You et al., 2017): Northeast China (NEC), North China (NC), Jiang-Huai (JH), South China (SC), Southwest China (SWC), the Tibetan Plateau (TB), western Northwest China (WNC), and eastern Northwest China (ENC). All of China, encompassing the 8 subregions, was abbreviated as CN.

## 3. Methods

### 3.1. Heatwaves

Heatwaves can be defined in terms of either percentiles or fixed thresholds, employing maximum, minimum, or apparent temperature, and may be counted based on consecutive days in which conditions are above the threshold defined (Chen and Zhai, 2017b Perkins and Alexander, 2013 Perkins et al., 2012). Much attention has been focused on daytime heatwaves (Li et al., 2019 Luo and Lau, 2017 Mazdiyasni and AghaKouchak, 2015 Meehl and Tebaldi, 2004 Russo et al., 2015). In this study, we defined a heatwave as an event during which the daily maximum temperature $T_{max}$ exceeded the daily relative threshold $T_d$ for at least 3 consecutive days in the 1961–2017 study period.

The daily relative threshold $T_d$ at each station is the 90th percentile of the daily maximum temperature for a 31-day period, i.e., on a given day and 15 days before and after this day, from 1961 to 2017. Moreover, since heatwaves primarily occur in summer, the daily maximum temperature on this given day must exceed 25 °C for the definition of summer days (Tank and Konnen, 2003). The characteristics of a heatwave can be expressed in terms of duration ($D$) and severity ($S$). $D$ was defined as the number of consecutive days when the daily maximum temperature $T_{max}$ exceeded the daily relative threshold $T_d$; heatwaves have a $D$ of at least 3 consecutive days. A heatwave that is weak but long is no less influential than a heatwave that is strong but

short. This is similar to drought, where the definition refers to the drought severity index (Mirabbasi et al., 2011 Yevjevich, 1967). $S$ denotes the cumulative sum of the difference between the daily maximum temperature and the daily relative threshold over the duration of the heatwave.

$$S = \sum_{1}^{D} (T_{max} - T_d) \tag{1}$$

### 3.2. Copula functions

Referring to a class of functions that link joint distribution functions with their respective cumulative distribution functions, Copula functions are also known as connection functions(Sklar, 1973). For the Copula function of 2 variables, assuming $F_X(x)$ and $F_Y(y)$ are the cumulative distribution functions of random variables $X$ and $Y$, respectively, the joint distribution function of $X$ and $Y$ defined by the Copula function is:

$$F(x,y) = C(F_X(x), F_Y(y)) = C(u,v) \tag{2}$$

where $C(u,v)$ is a Copula function that connects $F_X(x)$ with $F_Y(y)$ to form a joint distribution of the two.

In order to construct the Copula function of a heatwave, we should first determine $F_D(d)$ and $F_S(s)$, the respective cumulative distribution functions of the $D$ and $S$ for the heatwave. Five commonly used cumulative distribution functions, i.e., the γ distribution function, the logarithmic normal distribution function, the normal distribution function, the Weibull distribution function, and the exponential distribution function, were selected to fit the distribution of the $D$ and $S$ for the heatwave. The parameters of each distribution function were obtained using the maximum likelihood estimate, and the Kolmogorov-Smirnov (KS) method was applied to test the goodness of fit for each distribution function in order to evaluate whether the empirical distribution function conformed to the selected theoretical distribution. The results revealed that among the 673 meteorological stations in China, 40% of them conformed to a normal distribution in terms of $D$, while the stations that conformed to other distributions were relatively scattered. Meanwhile, 61% of stations featured a logarithmic normal distribution in terms of $S$, all of which passed the significance test at the level of 0.1. Therefore, while constructing the Copula function of the heatwave, we used the normal cumulative distribution function to fit $D$ and the logarithmic normal cumulative distribution function to fit $S$.

In this study, the optimal distribution of heatwaves was determined by 5 functions, i.e., the Clayton Copula function, the Frank Copula function, the Gumbel Copula function, the Galambos Copula function, and the Plackett Copula function. The expressions and parameter ranges of the above 5 Copula functions are as follows (Table 2):

$C(u,v)$ is a two-dimensional Copula joint function; $\theta$ is a parameter of the Copula function; there is a clear relationship expression between the $\theta$ parameter of the common Copula and Kendall rank correlation coefficient $\tau$; and $\tau$ can be calculated by the following formula:

$$\tau = \frac{2}{n(n-1)} \sum_{i<j} sign[(u_i - u_j)(v_i - v_j)] \tag{3}$$

$$sign(\varphi) = \begin{cases} 1 & \varphi > 0 \\ 0 & \varphi = 0 \\ -1 & \varphi < 0 \end{cases}$$

where $sign(\varphi)$ is a sign function (Mirabbasi et al., 2011).

Based on the Akaike information criterion (AIC) method, the fitting degrees of various Copula distributions were tested:

$$AIC = -2lnL + 2k \tag{4}$$

where $L$ is the logarithmic sum of the values of the Copula density function at the original observation data point of the variable, and $k$ is the sum of the number of related parameters of the Copula function. The smaller the value of AIC, the higher the fitting degree of the Copula function.

### 3.3. Joint occurrence probability

The "or" and "and" joint occurrence probability are the 2 combinations that researchers are most interested in. The cumulative distribution functions of the $D$ and $S$ of the heatwave were assumed to be $F_D(d)$ and $F_S(s)$, respectively. Per the definition of the Copula function, if 1 of the 2 variables of a heatwave exceeds the given threshold, i.e., when $D > d$ or $S > s$, this heatwave belongs to the "or" joint occurrence probability (denoted as $P_I$), which is:

$$P(D > d \text{ or } S > s) = 1 - C[F_D(d), F_S(s)] \tag{5}$$

If the 2 variables of a heatwave simultaneously exceed the given threshold, i.e., when D $>$ $d$ and S $>$ $s$, this heatwave features the "and" joint occurrence probability (denoted as $P_{II}$), which can be defined as:

$$P(D > d \text{ and } S > s) = 1 - F_D(d) - F_S(s) + C[F_D(d), F_S(s)] \tag{6}$$

In this study, the value of $d$ (or $s$) is mainly determined by the return levels of selected return periods (20-yr, 50-yr, and 100-yr). If $D$ or $S$ exceeds the 20-yr, 50-yr, or 100-yr return level, its respective joint occurrence probability is either $P_{I\ 20}$, $P_{I\ 50}$, or $P_{I\ 100}$. If $D$ and $S$ both exceed the 20-yr, 50-yr, or 100-yr return level, the respective joint occurrence probability is either $P_{II\ 20}$, $P_{II\ 50}$, or $P_{II\ 100}$.

### 3.4. Joint return period

The return periods of a single variable can be calculated by the following equations:

$$T_D = \frac{N}{1 - F_D(d)} \tag{7}$$

$$T_S = \frac{N}{1 - F_S(s)} \tag{8}$$

where $T_D$ and $T_S$ are the return periods of $D$ and $S$, respectively, and $N$ is

**Table 2**
Five Copula functions and their attributes.

| Copula function | Copula distribution function $C(u,v)$ | Parameter range |
|---|---|---|
| Clayton | $C(u,v) = (u^{-\theta} + v^{-\theta} - 1)^{-1/\theta}$ | $\theta \geq 0$ |
| Frank | $C(u,v) = -\frac{1}{\theta}\ln\left(1 + \frac{(e^{-\theta u}-1)(e^{-\theta v}-1)}{e^{-\theta}-1}\right)$ | $\theta \neq 0$ |
| Gumbel | $C(u,v) = exp\left(-\left[(-\ln u)^{1/\theta} + (-\ln v)^{1/\theta}\right]^{\theta}\right)$ | $\theta \geq 1$ |
| Galambos | $C(u,v) = uve^{[(-\ln u)^{-\theta} + (-\ln v)^{-\theta}]^{-1/\theta}}$ | $\theta \geq 0$ |
| Plackett | $C(u,v) = \frac{1}{2}\frac{1}{\theta-1}\left\{1 + (\theta-1)(u+v) - [(1+(\theta-1)(u+v))^2 - 4\theta(\theta-1)uv]^{1/2}\right\}$ | $\theta \geq 0$ |

the average interval between heatwaves.

When $D > d$ or $S > s$, the joint return period was defined as:

$$T_{\mathrm{I}} = \frac{N}{1 - C[F_D(d), F_S(s)]} \tag{9}$$

When $D > d$ and $S > s$, the joint return period was defined as:

$$T_{\mathrm{II}} = \frac{N}{1 - F_D(d) - F_S(s) + C[F_D(d), F_S(s)]} \tag{10}$$

When it comes to the "and" joint occurrence probability, heatwaves with the 2 variables exceeding the given threshold at the same time exert the most serious impact. Thus, the "and" joint return period was thoroughly analyzed in this study.

Changes in the occurrence probability of heatwaves during different periods were compared based on relative changes.

In order to determine whether temperature increases in China slowed beginning in the late 1990s, the annual mean maximum temperature ($T_{MAX}$) anomalies were calculated, with the climatological mean annual $T_{MAX}$ taken as that of the period 1961–2017. The regional means were calculated via regional gridding and the area-weighted averaging method. A Mann–Kendall (MK) test for abrupt changes in time series was employed (Kendall, 1975 Mann, 1945).

## 4. Results

### 4.1. Characteristics of changes in annual $T_{MAX}$

From 1961 to 2017, the annual $T_{MAX}$ anomalies in China exhibited a significant overall increasing trend ($p < .05$) of 0.24 °C/decade (Fig. 2a). For the period 1961–1997, the warming rate of $T_{MAX}$ was 0.12 °C/decade ($p < .05$), which was half that of 1961–2017. Annual

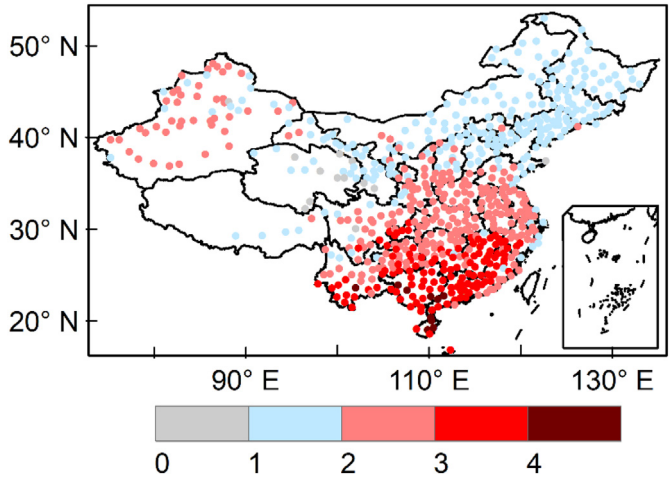


**Fig. 3.** Distribution of average occurrence number of summertime heatwaves in China from 1961 to 2017.

$T_{MAX}$ did not change significantly from 1998 to 2017, increasing at a rate of only 0.08 °C/decade. Fig. 2b shows the result of the MK abrupt change test for the annual $T_{MAX}$ from 1961 to 2017. An intersection point between the UF and UB curves was detected in 1996 and was significant at the confidence level of 95%. Before the abrupt change point, the annual $T_{MAX}$ was relatively cool; from the end of the 1990s to 2017, however, the annual $T_{MAX}$ was relatively warm.

Moving trend analysis was performed to further examine the characteristics of change in annual $T_{MAX}$ during different periods (Fig. 2c). The end year of the time series subjected to the moving trend analysis

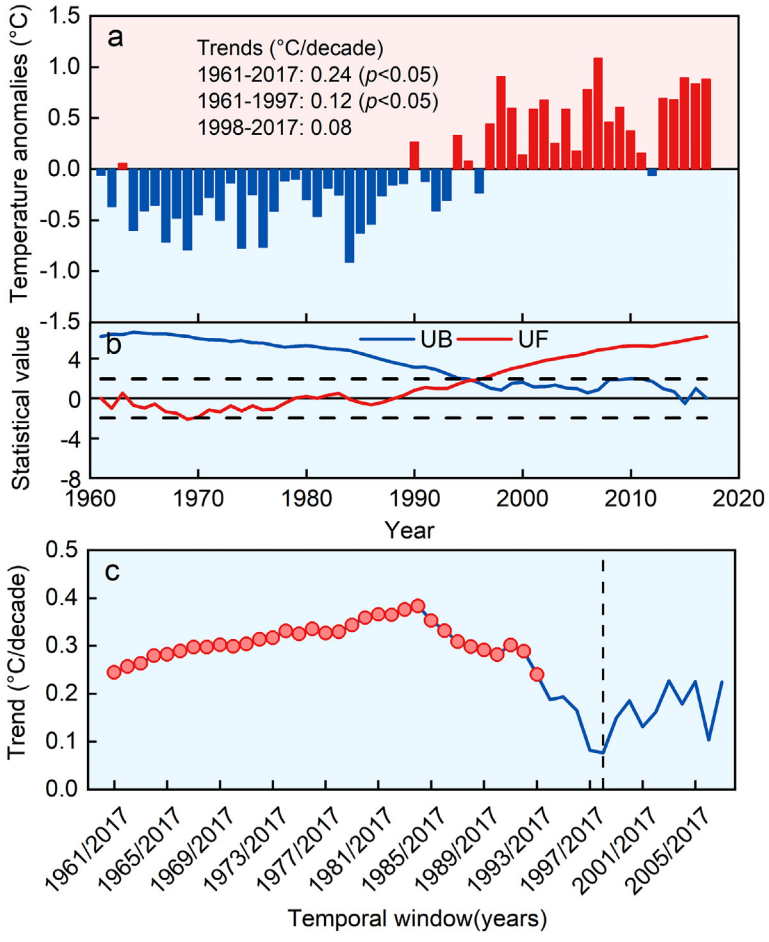


**Fig. 2.** (a) Annual mean time series of $T_{MAX}$ in China during 1961–2017; (b) Mann–Kendall test for the annual $T_{MAX}$ for the period 1961–2017 in China; (c) Moving trends of annual $T_{MAX}$ in a varied time window (the time window progressively narrows from 1961 to 2017 to 2007–2017).
The red dots represent years with significant trends ($p < .05$).

was fixed at 2017 while the start year was 1961, after which the start year of the time window gradually advanced toward the end year, i.e., 1961–2017, 1962–2017, …, 2007–2017. The increasing trend of annual $T_{MAX}$ in China became more pronounced with the narrowing of the time window until the start year reached 1984, after which the increasing trend gradually diminished. In particular, the increasing trend has been the weakest since 1998. It is thus interesting to examine how heatwaves have changed in China since the start of the warming slowdown in 1998.

Fig. 3 shows the average occurrence number of summertime heatwaves in China during 1961–2017. Heatwaves occurred most frequently in southern China, with an average of 3–4 times each year in the southern part of Southwest China and most of South China. The highest average annual number of heatwaves, i.e., > 4, was found in the southernmost parts of China. Heatwaves occurred least frequently in Northeast China, North China, and eastern Northwest China, with an average of 1–2 times each year. There were average of 2–3 summertime heatwaves in other parts of China, with the exception of the Qinghai-Tibet Plateau.

### 4.2. Different marginal return levels of univariate heatwaves

By calculating the correlation coefficients of *D* and *S* for the heatwaves in China during 1961–2017, we discovered a good correlation between the *D* and *S* values at all stations. Correlation coefficients for all but 4 stations were found to be significant at the 99% confidence level. The high correlation between the *D* and *S* of heatwaves in China indicates that the Copula function can be used to construct the joint distribution of heatwave variables. Therefore, the Copula function was applied to construct a joint distribution model of the characteristic variables of heatwaves in China and test the fitting degree of the Copula distribution of heatwaves detected at various meteorological stations. The results revealed that the minimum AIC value at 80% of the meteorological stations, i.e., 539 stations, corresponded to the Frank Copula function. This implies the symmetrical joint distribution of the *D* and *S* for heatwaves in China. The distribution characteristics can be accurately described by the Copula function connected by 2 cumulative distribution functions, namely the normal distribution function and the logarithmic normal distribution function.

Based on the definition of the return period, the normal distribution function and the logarithmic normal distribution function were used to fit the 20-yr, 50-yr, and 100-yr return levels of the *D* and *S* of heatwaves in China during 3 periods, i.e., 1961–2017, 1961–1997, and 1998–2017.

From the spatial distribution of the variable *D* of heatwaves with various return levels in different periods, it was found that the return level of *D* gradually increased from north to south, which is basically consistent with the occurrence number distribution of heatwaves. From 1961 to 2017, the maximum value of the 20-yr return level of *D* (7–10 d) mainly occurred in Jiang-Huai, South China, and Southwest China. The minimum value of the 20-yr return level of *D* (5–7 d) occurred in most parts of Northeast China, as well as parts of western North China and Northwest China (Fig. 4a). From 1961 to 1997, the 20-yr return level of *D* that was < 7.0 d covered a larger area in Northeast China, North China, Northwest China, and western Southwest China than during the other 2 periods, particularly in western Northeast China and a section of the southwest regions in eastern Northwest China, where the 20-yr return level of *D* was < 5.0 d (Fig. 4b). The 20-yr return level of *D* decreased 1.0–2.0 d in most parts of China from 1961 to 1997, although it remained unchanged in Jiang-Huai compared with the entire study period of 1961–2017. During the warming slowdown period, the 20-yr return level of *D* that was > 7.0 d covered 53% of the stations in China, more than the entire period (1961–2017) (45%) and the warming acceleration period (1961–1997) (33%). West China and northern North China witnessed a increase in the 20-yr return level of *D*, while the 20-yr return level of *D* decreased by approximately 1.0 d in Jiang-Huai and remained almost unchanged in Northeast China (Fig. 4c).

During the 3 periods, the 50-yr and 100-yr return levels of *D* were about 1.0 d longer than the 20-yr return level of *D*, with the spatial distribution being basically consistent. There was, however, a difference of < 1.0 d between the 50-yr and 100-yr return levels of *D* (Fig. 4d–i). There was no significant difference between the variable *D* of heatwaves with various return levels, which may be related to the insignificant difference between the historical *D* values of the heatwaves at each station.

Throughout the 3 periods, the spatial distributions of *D* and *S* for heatwaves with different return levels tended to be relatively consistent in most regions, although *S* varied greatly among the different periods. For the spatial distribution of the heatwave *S* with a 20-yr return level from 1961 to 2017, the minimum 20-yr return level of *S* (< 20.0 °C) was found in most of Northwest China, the eastern part of North China, the southern part of Southwest China, and South China coastal areas, while the minimum 20-yr return level of *S* in Jiang-Huai, South China, and parts of Southwest China was > 25.0 °C (Fig. 5a). From 1961 to 1997, the 20-yr return level of *S* in most regions of China was < 20.0 °C, with only the *S* of heatwaves in Jiang-Huai, the northern part of South China, and the eastern part of Southwest China exceeding 20.0 °C; the minimum 20-yr return level of *S* (< 10.0 °C) occurred in Southeast China coastal areas (Fig. 5b). During the period 1998–2017, the 20-yr return level of *S* was < 20.0 °C in a few regions, such as North China and Southeast China coastal areas, while in most other regions it was > 25.0 °C. Compared with 1961–2017 and 1961–1997, the 20-yr return level of *S* in various parts of China during 1998–2017 increased most noticeably, with the largest increase in Northeast China, followed by eastern Northwest China and Southwest China (Fig. 5c).

During all 3 periods, the 50-yr and 100-yr return levels of *S* were higher than the 20-yr return levels of *S*. From 1998 to 2017, the 20-yr, 50-yr, and 100-yr return levels of *S* surged more than they did during the periods 1961–2017 and 1961–1997 (Fig. 5d–i). Based on this analysis, after 1998—with the exception of Jiang-Huai—the return levels of *D* were growing in most regions, thus corresponding to longer return periods, although the increases were not as significant as those of the return levels of *S*.

Fig. 6 shows the probability density distributions of *D* and *S* for heatwaves with various return levels in China during the periods 1961–1997 and 1998–2017. It can be seen from the figure that compared with 1961–1997, the probability density distribution curves of the return levels of *D* and *S* in China during 1998–2017 shifted to the right, indicating that both the *D* and *S* of heatwaves with various return levels have increased since 1998. From 1961 to 1997, the probability of the average 20-yr return level of *D* (7.0 d) was 0.29. From 1998 to 2017, however, the distribution of the 20-yr return level of *D* became more concentrated, the number of heatwaves with a longer duration was higher, and the probability of the average 20-yr return level of *D* (7.6 d) was 0.35 (Fig. 5a). The probability density distributions of the *D* of heatwaves with 50-yr and 100-yr return levels were quite similar to that of the 20-yr return level of *D*. From 1998 to 2017, the average *D* of these 2 types of heatwaves increased by 0.5 d, while the return period of the extreme of duration heatwaves was getting shorter. If the *D* of heatwaves increased by 1.0 d, the heatwaves would become more extreme (Fig. 6b, c).

Compared with *D*, the 20-yr, 50-yr, and 100-yr return levels of *S* had relatively low probabilities, but the differences of extremes were greater for *S* with different return levels. Compared with the period 1961–1997, the distribution of *S* was relatively discrete during 1998–2017. The average of *S* with a 20-yr return level was 21.0 °C during 1961–1997, and increased by 8.0 °C to 29.0 °C during 1998–2017 (Fig. 6d). The probability density distributions of the *S* of heatwaves with 50-yr and 100-yr return levels were similar to that of the 20-yr return level, but the dispersion degree was greater. The average *S* of heatwaves with 50-yr and 100-yr return levels increased by

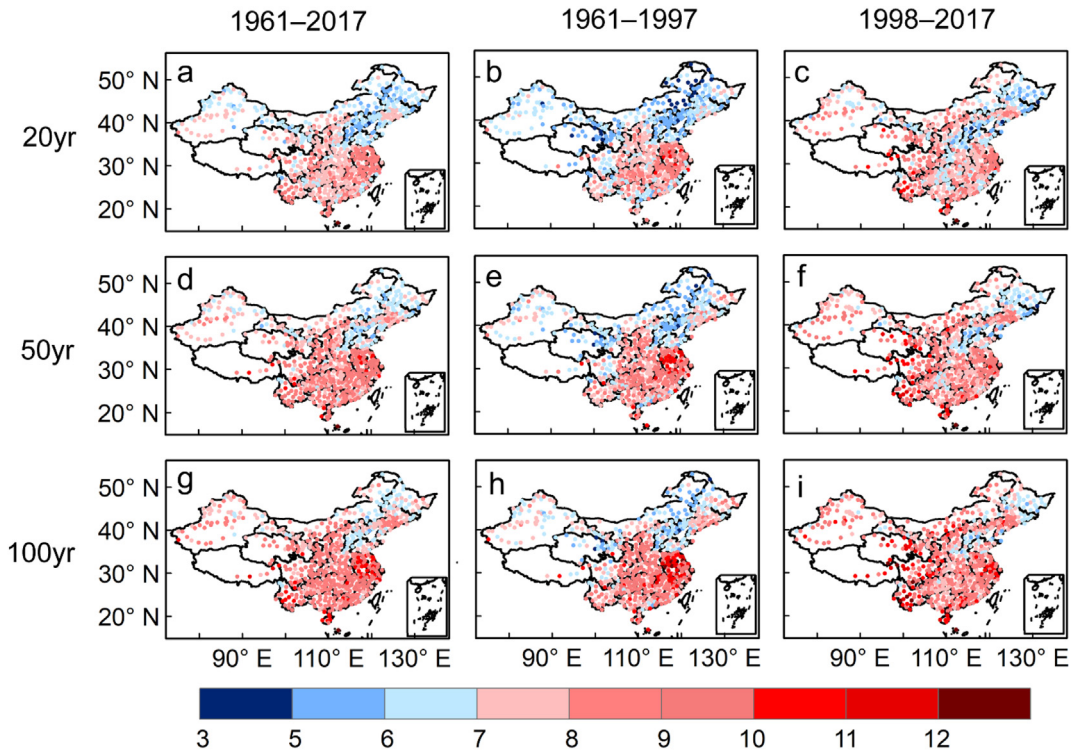


**Fig. 4.** Distribution of duration (*D*) of heatwaves with various return levels in different periods (unit: d).
Column: left: 1961–2017 (a, d, g); middle: 1961–1997 (b, e, h); right: 1998–2017 (c, f, i).
Row: top: 20-yr return (a, b, c); middle: 50-yr return (d, e, f); bottom: 100-yr return (g, h, i).

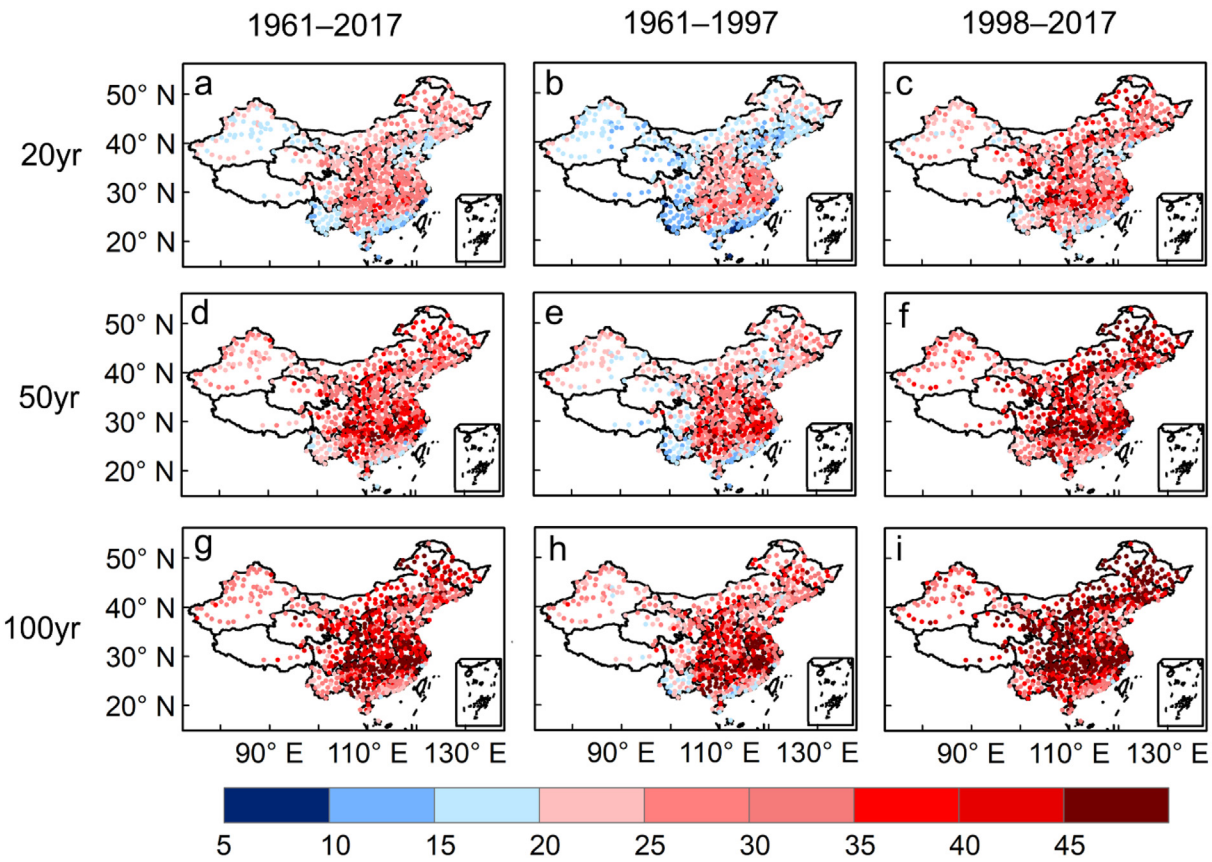


**Fig. 5.** Distribution of severity (*S*) of heatwaves with various return levels in different periods (unit:°C).
Column: left: 1961–2017 (a, d, g); middle: 1961–1997 (b, e, h); right: 1998–2017 (c, f, i).
Row: top: 20-yr return (a, b, c); middle: 50-yr return (d, e, f); bottom: 100-yr return (g, h, i).

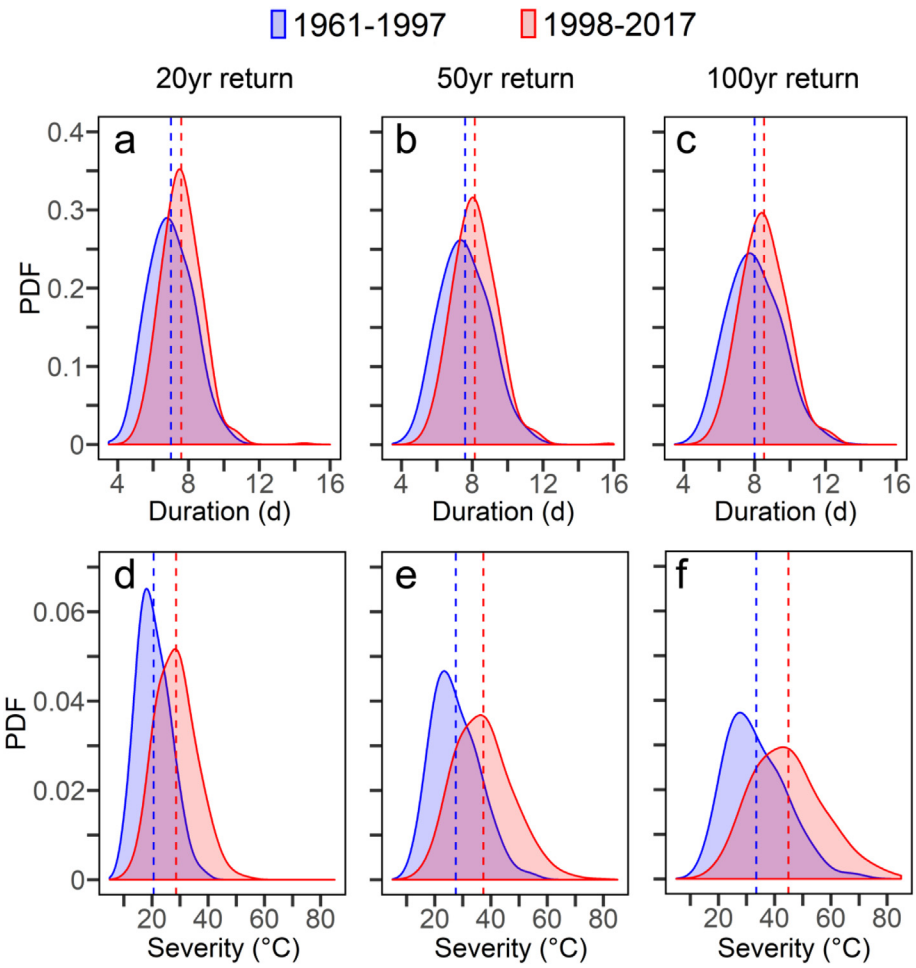


**Fig. 6.** Probability density distributions of duration (*D*) and severity (*S*) of heatwaves with various return levels in different periods. *D*: (a, b, c), *S*: (d, e, f); left: 20-yr return (a, d), middle: 50-yr return (b, e), right: 100-yr return (c, f). The blue and red dotted lines denote the average *D*(*S*) during 1961–1997 and 1998–2017, respectively.

10.0 °C and 11.0 °C, respectively, indicating that since 1998, the return period of the extreme of *S* shortened more than that of *D*, and as the return period expanded, the amplitude of the return level of *S* increased as well (Fig. 6e, f).

### *4.3. Joint occurrence probability distribution of bivariate heatwaves with different return levels*

Based on different return levels of *D* and *S* during 1961–1997, i.e., 20-yr, 50-yr, and 100-yr, the joint occurrence probabilities $P_I$and $P_{II}$ of *D* and *S* during 1961–1997 and 1998–2017 were calculated, and the changes of $P_I$and $P_{II}$from 1998 to 2017 relative to those of 1961–1997 were compared. Fig. 7 shows the distributions of the changes in $P_{I\ 20}$, $P_{I\ 50}$, and $P_{I\ 100}$ during 1998–2017 relative to those during 1961–1997. From the figure, it can be seen that $P_{I\ 20}$, $P_{I\ 50}$, and $P_{I\ 100}$ during 1998–2017 were relatively large compared to those during 1961–1997. The longer the return period, the greater the increase in the amplitude of $P_I$. Throughout China, $P_{I\ 20}$ increased by < 1%, while $P_{I\ 50}$ and $P_{I\ 100}$ grew by 1% and 2%, respectively. $P_{I\ 100}$ in the Qinghai-Tibet Plateau exhibited the largest relative increase, i.e., 5%, followed by eastern Northwest China, where $P_{I\ 100}$ increased by 4%. In contrast, Jiang-Huai underwent almost no change, and the variation in South China was also relatively weak. The changes in Northeast China and Southwest China were relatively consistent, with the increase amplitudes of $P_{I\ 50}$ and $P_{I\ 100}$ gradually increasing as compared with that of $P_{I\ 20}$.

Compared with the period 1961–1997, the changes in $P_{II}$ of heatwaves in most regions of China were similar to the changes in $P_I$ during the period 1998–2017, although the relative increase in the amplitudes of $P_{II\ 50}$ and $P_{II\ 100}$ were even larger, and exhibited a region of slight decrease or no change which was greater than that of $P_I$. $P_{II\ 20}$, $P_{II\ 50}$, and $P_{II\ 100}$ displayed almost the same positive and negative distributions of relative changes, and exhibited relative increases of 3%, 8%, and 16% across all of China, respectively.

In terms of the changes in various regions, the average relative change of $P_{II\ 20}$ in most parts of China, with the exceptions of Jiang-Huai and South China, was in the range of 4–6%, with no significant regional differences. The regional differences between $P_{II\ 50}$ and $P_{II\ 100}$ gradually increased during the warming slowdown period. Moreover, at some meteorological stations in the Qinghai-Tibet Plateau, eastern Northwest China, the northern part of Northeast China, and Southwest China, $P_{II\ 50}$ and $P_{II\ 100}$ surged by more than 50%. In eastern Northwest China and Northeast China, $P_{II\ 100}$ increased by an average of approximately 30%. Meanwhile, $P_{II\ 20}$, $P_{II\ 50}$, and $P_{II\ 100}$ changed very little in Jiang-Huai and South China (Fig. 8).

A comparison of the relative changes in the joint occurrence probabilities $P_I$ and $P_{II}$ of Chinese heatwaves during the periods 1961–1997 and 1998–2017 revealed that the probability of both heatwave variables *D* and *S* exceeding the threshold during a given return level was greater than the probability of a single heatwave variable surpassing the threshold. The joint occurrence probability of a heatwave with both variables exceeding the 100-yr return level grew by 16% during 1998–2017.

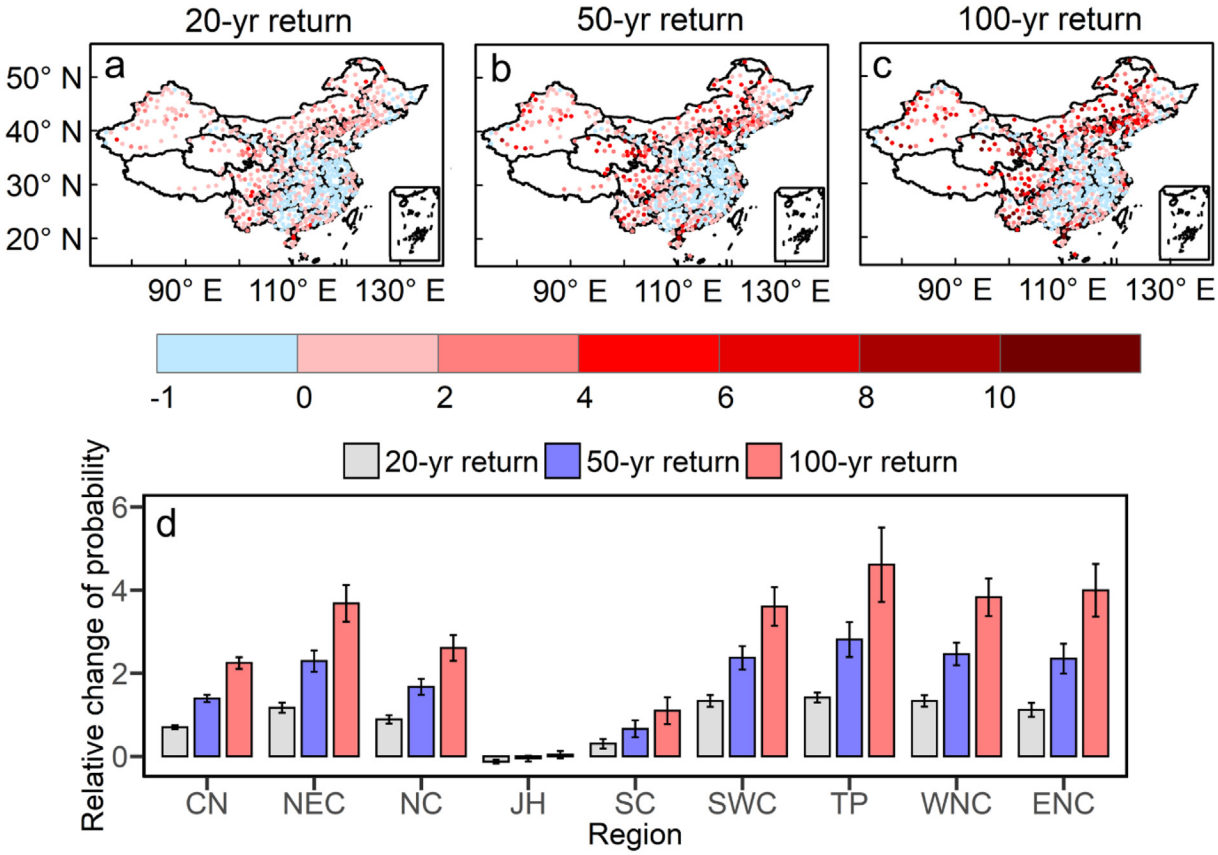


**Fig. 7.** (a) Distribution of relative changes of $P_{I\ 20}$ of heatwaves during 1998–2017 and 1961–1997; (b)-(c) as in (a) but for (b) $P_{I\ 50}$, (c) $P_{I\ 100}$; and (d) Relative changes of joint occurrence probability ($P_I$) heatwaves in the subregions during 1998–2017 and 1961–1997. Error bars represent the ensemble standard deviation.

### *4.4. Variation in the number of heatwave events exceeding joint return periods ($T_{II}$) of 20–100 years*

Based on the above analysis, $P_{II}$, i.e., the joint occurrence probability of bivariate heatwaves, exhibited a larger relative change from 1998 to 2017 than that during the period 1961–1997. Comparing the number of $T_{II}$ > 20-yr, > 50-yr, and > 100-yr across China during the periods 1961–1997 and 1998–2017 (Fig. 9), we found that the median number of heatwaves with $T_{II}$ > 100-yr during the period 1961–1997 was similar to that of heatwaves with $T_{II}$ > 50-yr. This implied that once an extreme heatwave with a return period of more than 20 years occurred, it was likely to have a return period of more than 100 years during the period 1961–1997. After 1998, there were more heatwaves with $T_{II}$ > 50-yr, and the median numbers of heatwaves with $T_{II}$ > 20-yr and > 100-yr were not much different from those during the period 1961–1997, indicating that after 1998, heatwaves with a $T_{II}$ of 50–100 years contributed more to the increase in the number of extreme heatwaves throughout China.

Based on the changes in the number of heatwave events exceeding different return periods in various subregions (Fig. 10), although the average annual number of heatwaves was the highest in South China for the 1961–2017 study period, the number of heatwaves in Jiang-Huai that exceeded the joint return period from 20 to 100 years during the period 1961–1997 was larger than that in other regions. For the heatwaves with $T_{II}$ > 20-yr in eastern Northwest China, the return period was mostly > 50-yr. After 1998, the number of extreme heatwaves with return periods ranging from 20 to 100 years fell drastically in Jiang-Huai, while the number of heatwaves with $T_{II}$ of 50–100 years slightly decreased in South China. As for other regions, the number of heatwaves with $T_{II}$of 20–100 years was greater in the 1998–2017 period compared to the 1961–2017 period, with the largest increase in amplitude found in Northeast China, eastern Northwest China, and the Qinghai-Tibet Plateau.

## 5. Discussion and conclusions

In this study, the Copula function was used to connect the duration and severity of heatwaves in China from 1961 to 2017, and to comprehensively evaluate the return levels and joint occurrence probability changes of univariate and bivariate heatwaves with different return periods against different climate change backgrounds (i.e., the warming acceleration period and the warming slowdown period). From the warming acceleration period (1961–1997) to the warming slowdown period (1998–2017), the return levels of heatwave duration increased by < 1.0 d as the return period increased. However, as the return period lengthened, the return level of heatwave severity rose as well, and the number of heatwaves exceeding the 50-yr joint return period increased. Moreover, the increased extreme heatwaves were dominated by heatwaves with joint return periods of 50–100 years, and as the joint occurrence probability of heatwaves with both variables exceeding the 100-yr return level grew by 16% across all of China, the heatwave extremity strengthened.

With the exceptions of Jiang-Huai and South China, all other regions have experienced an increase in the number of heatwaves. Since the beginning of the 1990s, the decreasing tendency of solar radiation has either decelerated or reversed in most regions of the world; hence, this shift has been described as a change from “dimming” to “brightening” (Wild, 2012 Wild et al., 2005). The dimming and brightening over China were likely due to the increase in absorptive and scattering aerosols in the atmosphere, respectively (Zhang et al., 2013). Increased

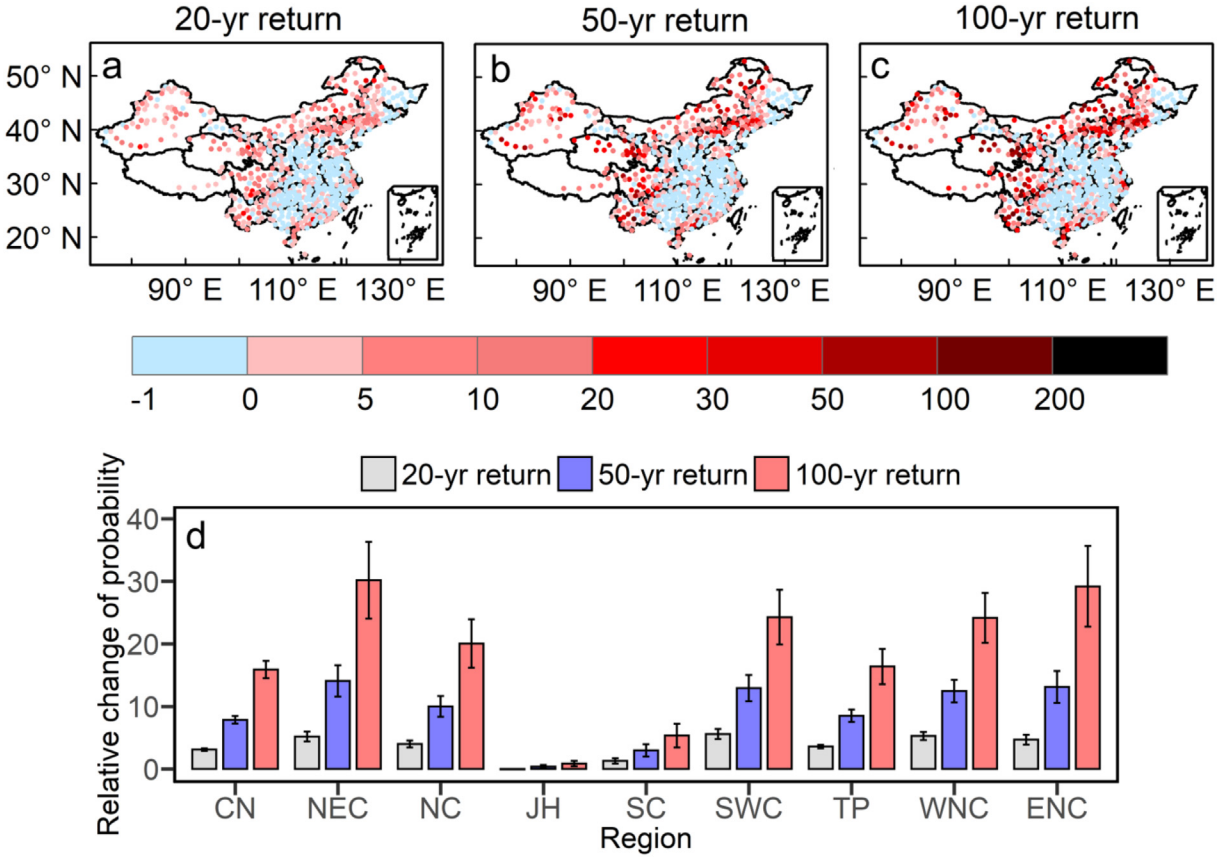


**Fig. 8.** (a) Distribution of relative changes of $P_{II\ 20}$ of heatwaves during 1998–2017 and 1961–1997; (b)-(c) as in (a) but for (b) $P_{II\ 50}$, (c) $P_{II\ 100}$; and (d) Relative changes of joint occurrence probability ($P_{II}$) of heatwaves in the subregions during 1998–2017 and 1961–1997.
Error bars represent the ensemble standard deviation.

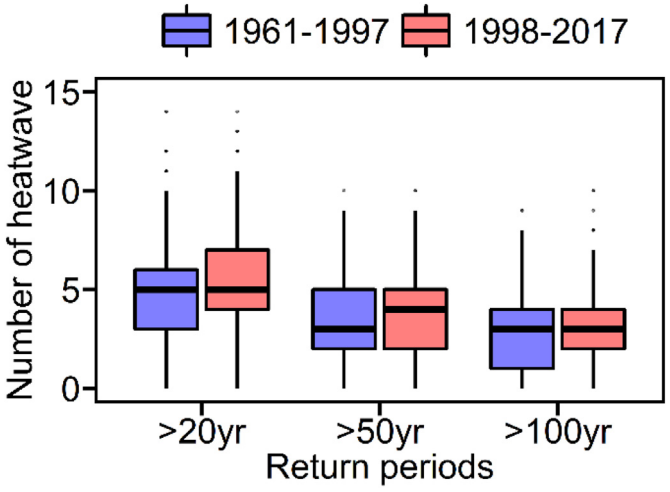


**Fig. 9.** Number of heatwave events exceeding different joint return periods in China during 1998–2017 and 1961–1997.
Blue represents the number of heatwaves during 1961–1997 and red denotes the number during 1998–2017. The black line in the middle of the box represents the median, the upper and lower borders of the box represent the upper and lower quartiles, respectively, the outermost edges connected by the solid line represent the 95th–5th percentiles, and a black dot denotes an outlier.

solar radiation is one of the major factors leading to temperature rise in summer, which further magnifies climate warming during this season (Sun et al., 2019). The transportation of water vapor to the north by southwest monsoon and the expansion of western Pacific Subtropical High results in the anomalous sinking of the airflow and relatively low humidity, the combined effect of which is likely to increase air temperatures in the lower troposphere of Jiang-Huai and South China (Chen and Lu, 2015), thus making these areas more prone to heatwaves than other areas on average. Nevertheless, with the correlation between the duration and severity of heatwaves being weaker than in other areas, these 2 regions have proven to be the most sensitive to the climate-warming slowdown (Chen and Zhai, 2017a). After 1998, the different return levels of heatwave durations in Jiang-Huai decreased compared with previous periods, and the number of extreme heatwaves was lower as well, although there was almost no change in South China. Natural variability and anthropogenic forcing were possible reasons for the fewer summertime heatwaves in these regions (Wang et al., 2014). The recent warming in the tropical Pacific, especially the warming associated with the tropical inter-decadal to multi-decadal variability centered over the central and eastern Pacific, could lead to excessive rainfall in eastern China (Li et al., 2010). The displacement of the Asian jet stream toward the equator in summer, as well as changes in the stratospheric temperatures, could also lead to the cooling of surface temperatures in eastern China (Wang et al., 2013 Yu et al., 2004). In addition, the increases in aerosols and cloudiness reduce solar radiation, causing extra cooling during the day in eastern China (Chen and Jeong, 2018 Li et al., 2015 Zhang et al., 2013).

The eastern Northwest China and the Qinghai-Tibet Plateau have witnessed increased solar radiation, and the Qinghai-Tibet Plateau was only slightly affected by climate-warming slowdown (Li et al., 2015 Sun et al., 2018). After 1998, the heatwaves became more extreme. Snow cover on the Qinghai-Tibet Plateau has significantly declined since 1995, which has contributed to the decrease of soil moisture in spring and summer, and thereby increased the occurrence probability of

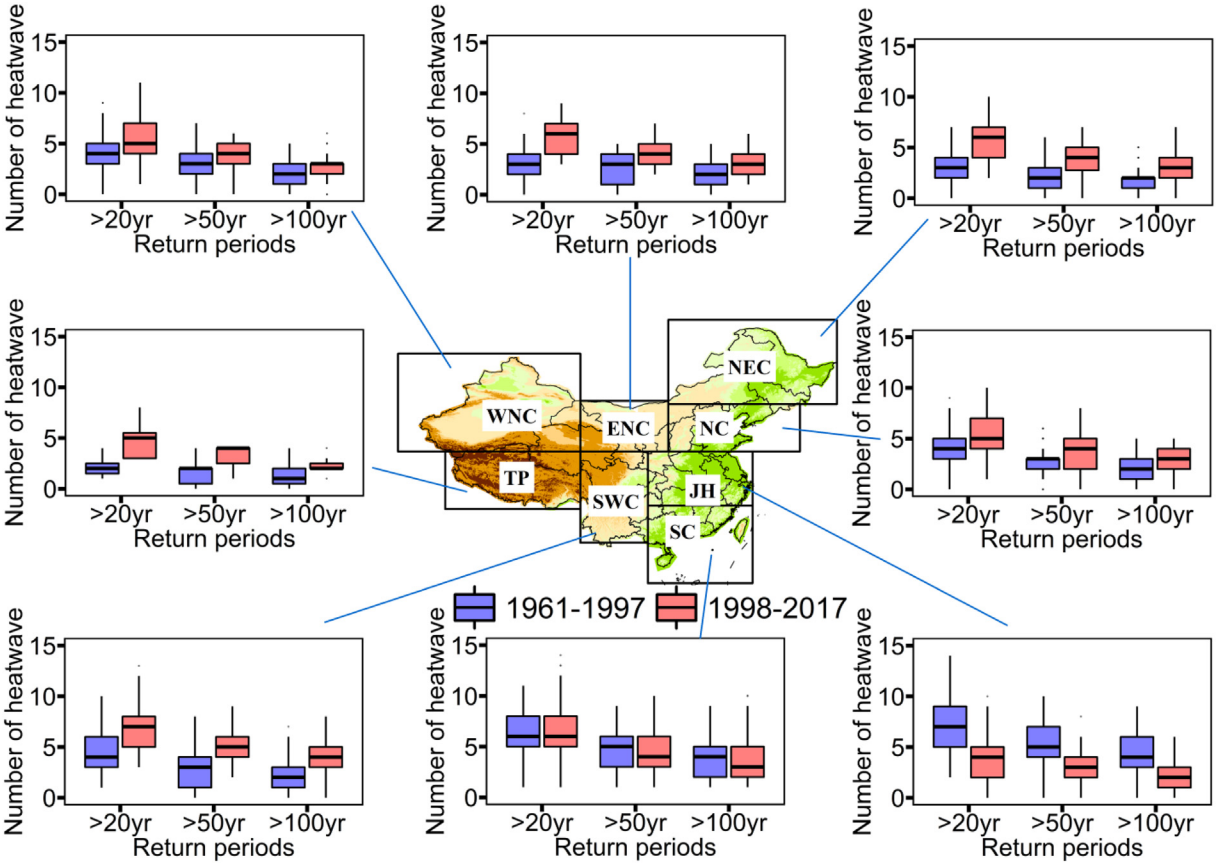


**Fig. 10.** Number of heatwave events exceeding different joint return periods in the subregions of China during 1998–2017 and 1961–1997. Blue represents the number of heatwaves during 1961–1997 and red denotes the number during 1998–2017. The black line in the middle of the box represents the median, the upper and lower borders of the box represent the upper and lower quartiles, respectively, the outermost edges connected by the solid line represent the 95th–5th percentiles, and a black dot denotes an outlier.

heatwaves (Wu et al., 2012a Wu et al., 2012b). Studies from other regions indicate that insufficient soil moisture will increase the frequency and duration of high-temperature heatwaves (Hirschi et al., 2010 Mueller and Seneviratne, 2012 Seneviratne et al., 2010).

Strong signals of human activities at different spatial scales can be detected during the variation of some extreme climate events (Yin and Sun, 2018). In particular, affected by rapid urbanization, the number of days with maximum temperatures > 25 °C measured by most meteorological stations in north-central China has significantly surged. The urbanization effect on the trend of summer days is 0.60–1.5 d/10 yr, with the largest urbanization contribution to the overall trend reaching 50% during 1961–2008 (Ren and Zhou, 2014). The apparent influence of urbanization might be one of the important reasons for the increased return levels of duration and severity of summer heatwaves detected by most meteorological stations in north-central China since 1998.

Therefore, under the combined effects of natural climate variability and human activities at various scales, the heatwaves in most parts of China became increasingly extreme during the warming slowdown period. In addition, the probability of bivariate heatwaves exceeding the extreme threshold increased, the duration and severity of heatwaves in urban areas experienced greater growth, and the risk of heatwaves rose.

## Declaration of Competing Interest

We declare that we have no financial and personal relationships with other people or organizations that can inappropriately influence our work, there is no professional or other personal interest of any nature or kind in any product, service and/or company that could be construed as influencing the position presented in, or the review of, the manuscript entitled, “Change in the heatwave statistical characteristics over China during the climate warming slowdown”.

## Acknowledgments

This study was supported by the National Key R&D Program of China (2018YFA0605603), the Third Batch of Ningxia Youth Talents Supporting Program (TJGC2018043), the Ningxia Youth Top Talent Training Project, and the Natural Science Foundation of China (NSFC) (41575003).

## References

Baldwin, J.W., Dessy, J.B., Vecchi, G.A., Oppenheimer, M., 2019. Temporally compound heat wave events and global warming: an emerging hazard. Earth’s Future 7, 411–427.
Chen, X., Jeong, S.-J., 2018. Irrigation enhances local warming with greater nocturnal warming effects than daytime cooling effects. Environ. Res. Lett. 13 024005.
Chen, R., Lu, R., 2015. Comparisons of the circulation anomalies associated with extreme heat in different regions of Eastern China. J. Clim. 28, 5830–5844.
Chen, Y., Zhai, P., 2017a. Persisting and strong warming hiatus over eastern China during the past two decades. Environ. Res. Lett. 12, 104010.
Chen, Y., Zhai, P., 2017b. Revisiting summertime hot extremes in China during 1961-2015: Overlooked compound extremes and significant changes. Geophys. Res. Lett. 44, 5096–5103.
Cheng, L., Hoerling, M., AghaKouchak, A., Livneh, B., Quan, X.-W., Eischeid, J., 2016. How has human-induced climate change affected california drought risk? J. Clim. 29, 111–120.
Christidis, N., Jones, G.S., Stott, P.A., 2014. Dramatically increasing chance of extremely hot summers since the 2003 European heatwave. Nat. Clim. Chang. 5, 46–50.
Ding, T., Qian, W., Yan, Z., 2009. Changes in hot days and heat waves in China during 1961-2007. Int. J. Climatol. 1452–1462.
Fyfe, J.C., Meehl, G.A., England, M.H., Mann, M.E., Santer, B.D., Flato, G.M., Hawkins, E.,

Gillett, N.P., Xie, S.-P., Kosaka, Y., Swart, N.C., 2016. Making sense of the early-2000s warming slowdown. Nat. Clim. Chang. 6, 224–228.
Hirschi, M., Seneviratne, S.I., Alexandrov, V., Boberg, F., Boroneant, C., Christensen, O.B., Formayer, H., Orlowsky, B., Stepanek, P., 2010. Observational evidence for soil-moisture impact on hot extremes in southeastern Europe. Nat. Geosci. 4, 17–21.
Jeong, D.I., Sushama, L., Khaliq, M.N., Roy, R., 2014. A copula-based multivariate analysis of Canadian RCM projected changes to flood characteristics for northeastern Canada. Clim. Dyn. 42, 2045–2066.
Jones, B., Tebaldi, C., O'Neill, B.C., Oleson, K., Gao, J., 2018. Avoiding population exposure to heat-related extremes: demographic change vs climate change. Clim. Chang. 146, 423–437.
Kao, S.-C., Govindaraju, R.S., 2008. Trivariate statistical analysis of extreme rainfall events via the Plackett family of copulas. Water Resour. Res. 44.
Kendall, M.G., 1975. Rank Correlation Measures. Charles Griffin.
Li, H., Dai, A., Zhou, T., Lu, J., 2010. Responses of East Asian summer monsoon to historical SST and atmospheric forcing during 1950–2000. Clim. Dyn. 34, 501–514.
Li, Q., Yang, S., Xu, W., Wang, X.L., Jones, P., Parker, D., Zhou, L., Feng, Y., Gao, Y., 2015. China experiencing the recent warming hiatus. Geophys. Res. Lett. 42, 889–898.
Li, X., You, Q., Ren, G., Wang, S., Zhang, Y., Yang, J., Zheng, G., 2019. Concurrent droughts and hot extremes in Northwest China from 1961 to 2017. Int. J. Climatol. 39, 2186–2196.
Luo, M., Lau, N.-C., 2017. Heat Waves in Southern China: synoptic behavior, long-term change, and urbanization effects. J. Clim. 30, 703–720.
Luo, M., Lau, N., 2018. Increasing Heat stress in Urban areas of Eastern China: acceleration by urbanization. Geophys. Res. Lett. 45, 13060–13069.
Luo, M., Lau, N.-C., 2019. Characteristics of summer heat stress in China during 1979–2014: climatology and long-term trends. Clim. Dyn. 53, 5375–5388.
Luo, M., Ning, G., Xu, F., Wang, S., Liu, Z., Yang, Y., 2020. Observed heatwave changes in arid Northwest China: physical mechanism and long-term trend. Atmos. Res. 242, 105009.
Mann, H.B., 1945. Nonparametric tests against trend. Econometrica 13, 245–259.
Mazdiyasni, O., AghaKouchak, A., 2015. Substantial increase in concurrent droughts and heatwaves in the United States. Proc. Natl. Acad. Sci. 112, 11484–11489.
Mazdiyasni, O., Sadegh, M., Chiang, F., AghaKouchak, A., 2019. Heat wave intensity duration frequency curve: a multivariate approach for hazard and attribution analysis. Sci. Rep. 9, 14117.
Medhaug, I., Stolpe, M.B., Fischer, E.M., Knutti, R., 2017. Reconciling controversies about the 'global warming hiatus'. Nature 545, 41–47.
Meehl, G.A., Tebaldi, C., 2004. More intense, more frequent, and longer lasting heat waves in the 21st century. Science 305, 994–997.
Mirabbasi, R., Fakheri-Fard, A., Dinpashoh, Y., 2011. Bivariate drought frequency analysis using the copula method. Theor. Appl. Climatol. 108, 191–206.
Mora, C., Dousset, B., Caldwell, I.R., Powell, F.E., Geronimo, R.C., Bielecki, Coral R., Counsell, C.W.W., Dietrich, B.S., Johnston, E.T., Louis, L.V., Lucas, M.P., McKenzie, M.M., Shea, A.G., Tseng, H., Giambelluca, T.W., Leon, L.R., Hawkins, E., Trauernicht, C., 2017. Global risk of deadly heat. Nat. Clim. Chang. 7, 501–506.
Mueller, B., Seneviratne, S.I., 2012. Hot days induced by precipitation deficits at the global scale. Proc. Natl. Acad. Sci. 109, 12398–12403.
Perkins, S.E., Alexander, L.V., 2013. On the measurement of heat waves. J. Clim. 26, 4500–4517.
Perkins, S.E., Alexander, L.V., Nairn, J.R., 2012. Increasing frequency, intensity and duration of observed global heatwaves and warm spells. Geophys. Res. Lett. 39.
Ren, G., Zhou, Y., 2014. Urbanization effect on trends of extreme temperature indices of national stations over mainland China, 1961–2008. J. Clim. 27, 2340–2360.
Russo, S., Sillmann, J., Fischer, E.M., 2015. Top ten European heatwaves since 1950 and their occurrence in the coming decades. Environ. Res. Lett. 10, 124003.
Russo, S., Sillmann, J., Sippel, S., Barcikowska, M.J., Ghisetti, C., Smid, M., O'Neill, B., 2019. Half a degree and rapid socioeconomic development matter for heatwave risk. Nat. Commun. 10, 136.
Seneviratne, S.I., Corti, T., Davin, E.L., Hirschi, M., Jaeger, E.B., Lehner, I., Orlowsky, B., Teuling, A.J., 2010. Investigating soil moisture–climate interactions in a changing climate: a review. Earth Sci. Rev. 99, 125–161.
Shiau, J.T., Modarres, R., 2009. Copula-based drought severity-duration-frequency analysis in Iran. Meteorol. Appl. 16, 481–489.
Sklar, A., 1973. Random variables, joint distribution functions, and copulas. Kybernetika 9, 449–460.
Sun, Y., Zhang, X., Zwiers, F.W., Song, L., Wan, H., Hu, T., Yin, H., Ren, G., 2014. Rapid increase in the risk of extreme summer heat in Eastern China. Nat. Clim. Chang. 4, 1082–1085.
Sun, X., Ren, G., Ren, Y., Fang, Y., Liu, Y., Xue, X., Zhang, P., 2018. A remarkable climate warming hiatus over Northeast China since 1998. Theor. Appl. Climatol. 133, 579–594.
Sun, X., Li, S., Liu, B., 2019. Comparative analysis of the mechanisms of intensified summer warming over Europe – West Asia and Northeast Asia since the Mid-1990s through a Process-based decomposition method. Adv. Atmos. Sci. 36, 1340–1354.
Tank, A.M.G.K., Konnen, G.P., 2003. Trends in indices of daily temperature and precipitation extremes in Europe, 1946–99. J. Clim. 16, 3665–3680.
Tebaldi, C., Lobell, D., 2018. Estimated impacts of emission reductions on wheat and maize crops. Clim. Chang. 146, 533–545.
Teuling, A.J., 2018. A hot future for European droughts. Nat. Clim. Chang. 8, 364–365.
Wang, X., Zhou, W., Wang, D., Wang, C., 2013. The impacts of the summer Asian Jet Stream biases on surface air temperature in mid-eastern China in IPCC AR4 models. Int. J. Climatol. 33, 265–276.
Wang, W., Zhou, W., Chen, D., 2014. Summer high temperature extremes in Southeast China: bonding with the El Niño–Southern Oscillation and East Asian Summer Monsoon coupled system. J. Clim. 27, 4122–4138.
Wang, J., Han, Y., Stein, M.L., Kotamarthi, V.R., Huang, W.K., 2016. Evaluation of dynamically downscaled extreme temperature using a spatially-aggregated generalized extreme value (GEV) model. Clim. Dyn. 47, 2833–2849.
Warshaw, C., 2018. Spatial variation in messaging effects. Nat. Clim. Chang. 8, 360–361.
Wehner, M., Stone, D., Mitchell, D., Shiogama, H., Fischer, E., Graff, L.S., Kharin, V.V., Lierhammer, L., Sanderson, B., Krishnan, H., 2018. Changes in extremely hot days under stabilized 1.5 and 2.0 C global warming scenarios as simulated by the HAPPI multi-model ensemble. Earth Syst. Dyn. 9, 299–311.
Wild, M., 2012. Enlightening global dimming and Brightening. Bull. Am. Meteorol. Soc. 93, 27–37.
Wild, M., Gilgen, H., Roesch, A., Ohmura, A., Long, C.N., Dutton, E.G., Forgan, B., Kallis, A., Russak, V., Tsvetkov, A., 2005. From dimming to brightening: Decadal changes in solar radiation at Earth's surface. Science 308, 847–850.
Wu, Z., Li, J., Jiang, Z., Ma, T., 2012a. Modulation of the Tibetan Plateau snow cover on the ENSO Teleconnections: from the East Asian Summer Monsoon perspective. J. Clim. 25, 2481–2489.
Wu, Z., Jiang, Z., Li, J., Zhong, S., Wang, L., 2012b. Possible association of the western Tibetan Plateau snow cover with the decadal to interdecadal variations of northern China heatwave frequency. Clim. Dyn. 39, 2393–2402.
Yan, J., 2006. Multivariate modeling with copulas and engineering applications. In: Handbook in Engineering Statistics. Springer, New York, United States.
Yang, C., Panmao, Z., Baiquan, Z., 2018. Detectable impacts of the past half-degree global warming on summertime hot extremes in China. Geophys. Res. Lett. 45, 7130–7139.
Yevjevich, V.M., 1967. An objective approach to definitions and investigations of continental hydrologic droughts. Hydrol. Pap. (Colorado State University) 23.
Yin, H., Sun, Y., 2018. Detection of anthropogenic influence on fixed threshold indices of extreme temperature. J. Clim. 31, 6341–6352.
You, Q., Jiang, Z., Kong, L., Wu, Z., Bao, Y., Kang, S., Pepin, N., 2017. A comparison of heat wave climatologies and trends in China based on multiple definitions. Clim. Dyn. 48, 3975–3989.
Yu, R., Wang, B., Zhou, T., 2004. Tropospheric cooling and summer monsoon weakening trend over East Asia. Geophys. Res. Lett. 31.
Zhang, H., Yin, Q., Nakajima, T., Makiko, N.M., Lu, P., He, J., 2013. Influence of changes in solar radiation on changes of surface temperature in China. Acta Meteorologica Sinica 27, 87–97.
Zhao, Y., Ducharne, A., Sultan, B., Braconnot, P., Vautard, R., 2015. Estimating heat stress from climate-based indicators: present-day biases and future spreads in the CMIP5 global climate model ensemble. Environ. Res. Lett. 10, 084013.
Zhou, P., Liu, Z., 2018. Likelihood of concurrent climate extremes and variations over China. Environ. Res. Lett. 13, 094023.